International Core Journal of Engineering Volume 12 Issue 5, 2026
ISSN: 2414-1895 DOI: 10.6919/ICJE.202605_12(5).0012

Simulation Study on Ultra-High Pressure Rupture Disc of Pressure-Controlled Testing Tool

Chao Chen[1], Yangyang Xu[2], Shijie Li[1], Xiaoqiang Wang[1]

[1] Sinopec Southwest Petroleum Engineering Co., Ltd. Well Service Branch, Deyang, Sichuan 618000, China

[2] School of Mechanical Engineering, Southwest Petroleum University, Chengdu, Sichuan 610500, China

Abstract

In APR formation testing technology, the ultra-high pressure rupture disc is a core component ensuring the reliability of downhole operations. Aiming at the requirements for performance optimization and precise design of rupture discs under ultra-high pressure downhole conditions, this study adopts Inconel 718 nickel-based alloy as the bursting disc material and establishes a three-dimensional simulation model with reference to the 17.5 ksi rupture disc of OSECO Corporation. The effects of initial thickness S0, arch height H, top thinning thickness t0 and temperature on the stress distribution and rupture characteristics of the bursting disc are systematically analyzed using simulation software. The results show that increasing the initial thickness and arch height can reduce the degree of stress concentration and improve the burst pressure; the top thinning structure can transfer the stress concentration zone from the arch base to the arch crown to achieve controllable rupture, which is consistent with the actual failure morphology; the influence of temperature on burst pressure is mainly reflected by the attenuation of yield strength, and the fitted temperature-burst pressure curve agrees well with the trend of similar products of OSECO. This study verifies the adaptability of Inconel 718 alloy and the rationality of structural design, providing a theoretical basis and technical support for the design optimization and engineering application of ultra-high pressure rupture discs.

Keywords

APR Testing Tool; Ultra-high Pressure Rupture Disc; Inconel 718; Numerical Simulation; Structural Optimization; Rupture Characteristics.

1. Introduction

APR formation testing is a core technology for reservoir evaluation. Testing instruments including circulation valves, packers and pressure measuring gauges are deployed to the target well interval through tubing. Downhole shut-in can be realized by regulating the circulation valve via annulus pressure without tripping the drill string, and formation parameters can be accurately acquired accordingly. Under normal operating conditions, the circulation valve triggers the rupture disc to open within a preset annulus pressure range. Fluid pressure is transmitted through the rupture channel to drive the mandrel downward, which subsequently opens the circulation port to achieve dual functions of downhole shut-in and circulating well killing. A rupture disc mainly consists of three core components: a threaded clamp ring, a sealing element and a bursting disc. When the system pressure reaches the rated threshold of the rupture disc, the internal bursting disc ruptures. During field service, the rupture disc connects the high-pressure annulus and low-pressure annulus, maintaining the

ISSN: 2414-1895 DOI: 10.6919/ICJE.202605_12(5).0012

annulus pressure within a safe range. The bursting disc is tightly welded to the clamp ring. Once ruptured under pressure, it exhibits a typical outward-expanding rupture morphology, forming a relief hole in the central region while the base material remains intact at the edge. The burst pressure of a rupture disc is jointly determined by the structural configuration and material properties of the internal bursting disc.

In petroleum drilling engineering, rupture disc technology is also applicable for pressure regulation in offshore oil and gas fields, acting as a critical approach for trapped annulus pressure control during offshore hydrocarbon development. Once the annulus pressure reaches the preset threshold, the rupture disc installed on the casing string ruptures to release pressure into the lower annulus. As a fundamental safety relief component for pressure-bearing fluid equipment, bursting discs have been developed and applied for more than 80 years, and were initially adopted for safety protection in the chemical industry. However, bursting discs assembled with APR tools serve in harsh downhole environments, where working conditions are far more severe than conventional service scenarios, imposing stringent requirements on material selection and structural design[1,2]. At present, existing research regarding the rupture behavior, stress evolution and performance characterization of bursting discs under ultra-high pressure and severe downhole conditions remains insufficient, and systematic design methodologies, testing criteria and comprehensive evaluation systems are yet to be perfected.

2. Theoretical Research on Ultra-High Pressure Bursting Discs of Rupture Discs

2.1 Structure and Working Principle of Bursting Disc

At present, research on ultra-high pressure bursting discs remains relatively insufficient. Combined with their practical application scenarios in pressure vessels, existing bursting discs can be classified from multiple perspectives. In terms of failure mode, they are categorized into tensile rupture type, triggered rupture type and detached type. In terms of loading mode, they are divided into shear type, bending type, tension type and compression type. In terms of structural configuration, they include flat type, forward domed type and reverse domed type. In terms of material property, they are classified into metallic and non-metallic types [3-6].

As illustrated in Fig. 1, the core component inside the rupture disc, namely the bursting disc, is divided into forward domed and reverse domed types according to structural morphology. The forward domed bursting disc, also known as the tension-type bursting disc, bulges from the inner end face to the outer end face of the rupture disc, with its arched surface exposed to the low-pressure region of the pressure system. The reverse domed bursting disc, referred to as the compression-type bursting disc, possesses an inverted arched structure. During installation, its arched surface faces the high-pressure region of the pressure system. Forward domed bursting discs can be further subdivided into plain type, slotted type and grooved type [1].

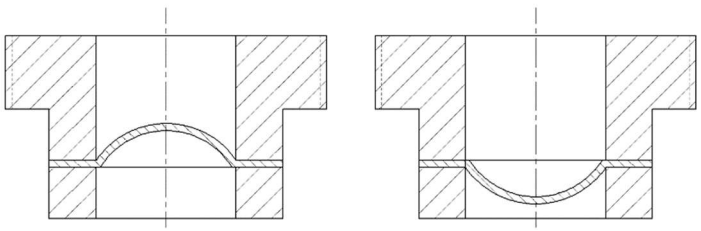

(a) Forward domed rupture disc (b) Reverse domed rupture disc

Fig. 1 Schematic diagram of common rupture disc classifications

The mainstream bursting disc adopted for rupture discs of APR tools is the plain forward domed type. When the operating pressure of a pressure vessel is lower than the design pressure of the bursting

ISSN: 2414-1895 DOI: 10.6919/ICJE.202605_12(5).0012

disc, only elastic deformation occurs without plastic strain. Once the operating pressure reaches and exceeds the design pressure threshold, the bursting disc enters the plastic deformation stage. If the pressure continues to rise to the ultimate strength of the material, the bursting disc will undergo rupture failure. Since the core component of the rupture disc matched with APR tools is the plain forward domed bursting disc, subsequent discussion will be mainly conducted on this type of bursting disc.

2.2 Calculation Methods of Burst Pressure

As the core pressure relief component of the rupture disc, the design burst pressure of the bursting disc directly determines the overall burst pressure characteristics of the rupture disc. The most widely applied formula for design pressure in engineering practice is presented as follows:

$$P_b = \frac{S_0 k}{d + 1.2R} \tag{1}$$

Where, S_0 is the initial thickness of the bursting disc, in m; k is the empirical engineering coefficient of the material, with values ranging from 1800 to 2000; d is the relief diameter of the bursting disc, in m; R is the fillet radius, in m.

A corresponding burst pressure formula for plain forward-domed bursting discs was derived via engineering calculation, as reported in the literature [7], given as:

$$P_b = \frac{K\sigma_b S_0}{d} \tag{2}$$

Where, K is the coefficient associated with the strain hardening degree of the material; σ_b is the ultimate strength of the material, which is obtained via experimental measurement in MPa and is severely affected by temperature.

Based on the spherical assumption in the forming process of bursting discs, Lake et al. adopted the constant-volume uniform thinning method to derive the geometric relationship of strain deformation, and further obtained the calculation formula for the design burst pressure of bursting discs[8]:

$$P_b = \frac{4\sigma_b S_0 h a_0^2}{(a_0^2 + h^2)^2} \tag{3}$$

Where, h is the arch height of the bursting disc, in mm; a_0 is the aperture of the bursting disc, in mm.

Jin et al. adopted the uniform thinning arc length method to construct the following geometric relationship for deformed bursting discs can be established as shown in [9]:

$$\varepsilon_i = \ln(1 + \frac{4h^2}{a_0^2}), \quad \sigma_i = \psi(\varepsilon_i) \tag{4}$$

Where, ε_i is the equivalent strain (dimensionless); σ_i is the equivalent stress, in MPa.

Meanwhile, the following calculation formula was derived based on the uniform-thickness thin-walled spherical shell membrane theory:

ISSN: 2414-1895 DOI: 10.6919/ICJE.202605_12(5).0012

$$P_b = \frac{\sigma_i S_0}{2a^2} \tag{5}$$

Although numerous calculation methods for the design burst pressure of bursting discs have been proposed by global researchers, most of these formulas are grounded in thin-walled spherical shell membrane theory or uniform-thickness spherical shell theory, leading to relatively obvious calculation errors. Moreover, studies concerning ultra-high pressure bursting discs with large thickness-diameter ratios remain scarce worldwide.

Furthermore, when establishing the theoretical system for bursting disc safety design in 1950, Hill indicated that the wall thickness of a bursting disc does not undergo uniform thinning during the forming process. Instead, the thickness presents a gradual decreasing trend from the center to the peripheral region of the circular blank, and its thickness-thinning path exhibits an arc-shaped profile [10]. Theoretically, precise control over the burst pressure of bursting discs can be realized by regulating the thickness-thinning law. On the basis of previous research achievements, subsequent scholars have further derived the burst pressure calculation expressions for grooved and slit-type bursting discs.

3. Research on Material Properties of Ultra-High Pressure Bursting Discs

Bursting discs adopted in rupture disc products manufactured by OSECO Corporation are fabricated from nickel-based superalloys. In this study, the wrought nickel-based high-temperature superalloy Inconel 718 was selected as the raw material for high-pressure bursting discs, and a systematic analysis of its material properties was conducted in accordance with the official technical data sheet of this alloy.Inconel 718 superalloy possesses excellent tensile strength, fatigue strength, creep resistance and fracture toughness. It exhibits outstanding resistance to stress corrosion cracking and pitting corrosion under both high-temperature and low-temperature service conditions. Within the temperature range below 650 °C, this alloy holds a leading level of yield strength among wrought high-temperature superalloys. Meanwhile, it features superior fatigue resistance, radiation resistance, oxidation resistance and corrosion resistance, as well as favorable process adaptability, weldability and long-term microstructural stability.

Table 1. Temperature-dependent mechanical properties of Inconel 718 superalloy

Temperature (°F)	Young's Modulus (GPa)	Yield Strength (MPa)
50	199.18	1071.52
100	198.08	1052.04
150	197.14	1036.92
200	196.32	1024.71
250	194.71	1015.87
300	193.07	1009.31
350	191.86	1002.03
400	190.30	995.78
450	188.61	992.03
500	186.86	988.18

ISSN: 2414-1895 DOI: 10.6919/ICJE.202605_12(5).0012

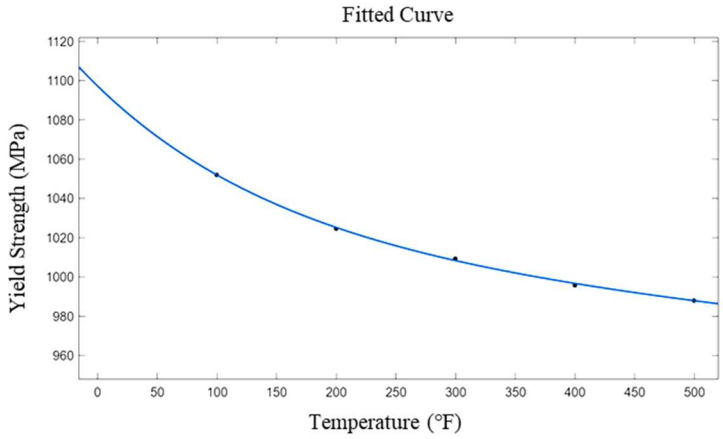

(a) Fitted curve of yield strength versus temperature

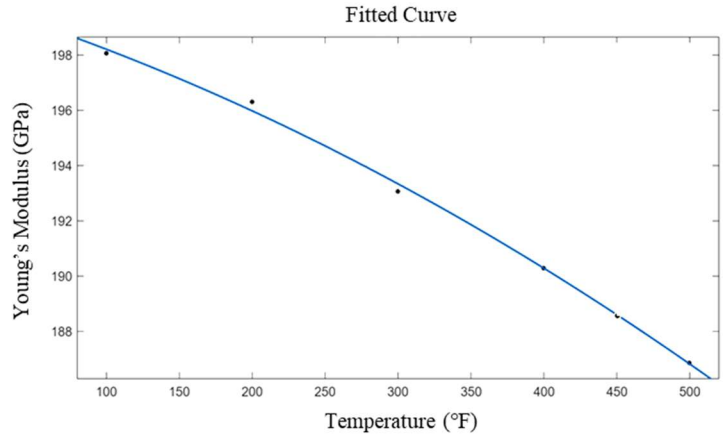

(b) Fitted curve of Young's modulus versus temperature

Fig. 2 Fitted temperature-dependent property curves of the material

In high-H_2S environments, the corrosion resistance of Inconel 718 is superior to that of 26$CrMo_4$s steel used for G105-grade drill pipes. The nickel element in this alloy has strong passivation capability and high intrinsic potential, with remarkable stability against halide ions. It can effectively inhibit chloride-induced stress corrosion cracking, and maintains excellent corrosion resistance in strong oxidizing environments, as well as diverse inorganic, organic and mixed acid-base media [11]. With reference to the material technical manual, the property parameters of annealed & precipitation-hardened Inconel 718 (standard heat treatment procedure: solution annealing + 8 h thermal holding at 720 °C + furnace cooling to 620 °C with 8 h thermal holding + air cooling) were obtained via parameter fitting, as presented in Table 1. Under this heat-treated state, the Young's modulus and yield strength of the alloy are significantly affected by temperature variation, while its Poisson's ratio is fixed at 0.305. Some of the data in the above table were acquired via parameter fitting, as shown in Fig. 2.

4. Model Establishment and Simulation Settings

4.1 Rupture Disc Model Establishment

The rupture disc model was established with reference to the 15.5K, 16K and 17.5K rupture disc samples produced by OSECO Corporation (Fig. 3). Among them, the 15.5K and 16K rupture discs have been burst tested, and their bursting discs present normal tearing failure characteristics.

ISSN: 2414-1895 DOI: 10.6919/ICJE.202605_12(5).0012

(a) Samples of 15.5K, 16K and 17.5K rupture discs

(b) Orthographic views of the 17.5K rupture disc

Fig. 3 Rupture disc samples from OSECO Corporation

As shown in the lower-left section of Fig. 3(b), faint welding traces are clearly observable. The diameter of the central relief hole in the rupture disc is 9.6 mm. The bursting disc experiences a certain thickness reduction after expansion, stretching and rupture, so it remains unclear whether the bursting disc is designed with a top-thinned structure. Accordingly, a detailed parametric discussion of the bursting disc is necessary.

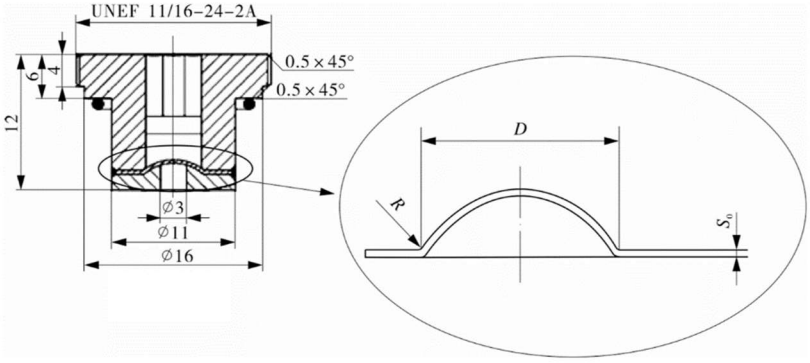

Fig. 4 Dimensions of casing rupture disc[12]

Fig. 4 presents the structure and dimensions of the rupture disc applied to casings. The main dimensions of the bursting disc involve thickness S_0, chamfer R and relief diameter D[13]. The pressure rating of this bursting disc is merely 30 MPa, necessitating further structural refinement for ultra-high pressure bursting discs. As illustrated in Fig. 5, a three-dimensional model of the 17.5K rupture disc was constructed using 3D design software. Parameters including the major diameter of the rupture

ISSN: 2414-1895 DOI: 10.6919/ICJE.202605_12(5).0012

disc, relief diameter, major diameter of the bursting disc D, local thinning thickness t_0, initial thickness S_0, inner fillet R_{inner}, outer fillet R_{outer}, and arch height H were defined for the simulation investigation.

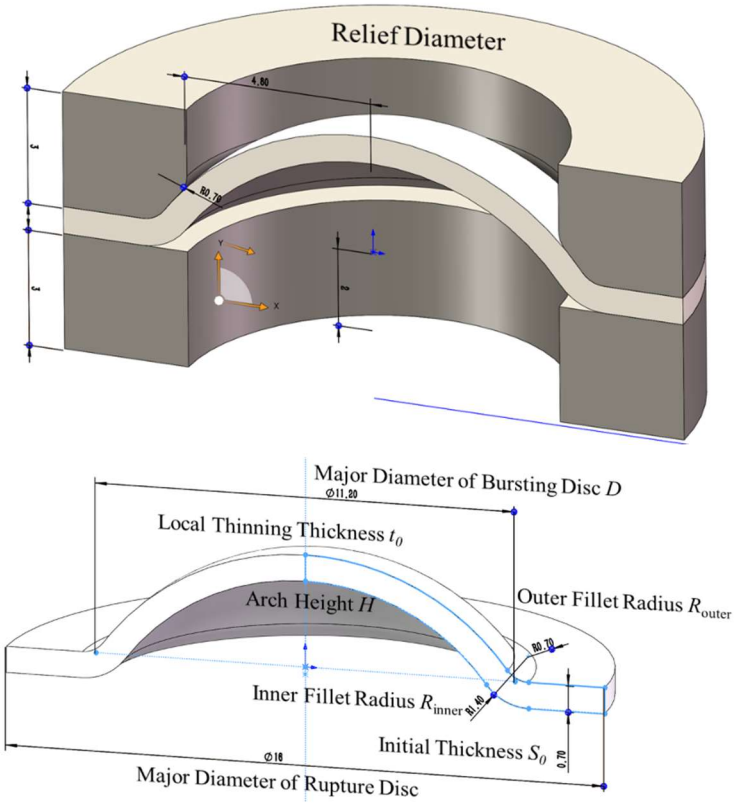

Fig.5 Structure of the 17.5K rupture disc

4.2 Simulation Settings for the Rupture Disc

As shown in Fig. 6, quadrilateral meshes are used for both the clamping zone and the bursting disc, and an advanced algorithm is employed for mesh generation. The global element size is set to 0.1 for the bursting disc and 0.2 for the clamping zone. Partitioning is applied to the upper and lower ends of the fillets to optimize the mesh distribution in these regions. The element type features hybrid formulation, constant pressure, reduced integration, and hourglass control.

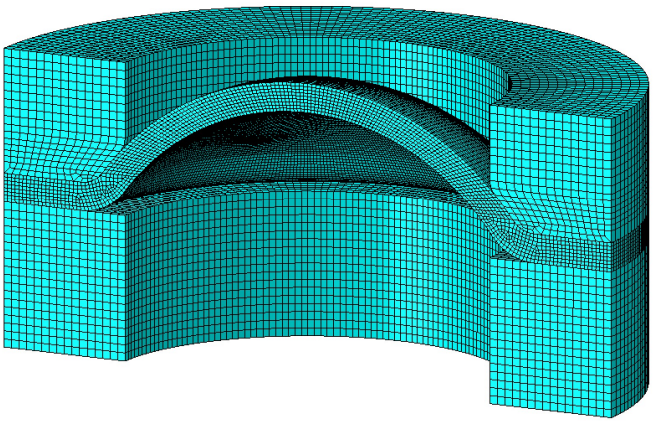

Fig. 6 Mesh Generation

ISSN: 2414-1895 DOI: 10.6919/ICJE.202605_12(5).0012

5. Mechanical Characteristic Analysis

5.1 Effect of Initial Plate Thickness S0 on Stress

Stress contours can intuitively reveal the overall stress distribution of the bursting disc. With other dimensional parameters kept constant, the influence of initial plate thickness S_0 on the stress distribution was investigated by controlling S_0. Four values of S_0 were adopted: 0.5 mm, 0.6 mm, 0.7 mm and 0.8 mm. The arch height H was fixed at 3 mm, the major diameter of the bursting disc D at 11.2 mm, no top thinning was applied, the outer fillet R_{outer} at 0.7 mm, and the inner fillet R_{inner} at 1.4 mm. The simulation results are shown in Fig. 7. It can be seen that when the bursting disc is subjected to pressure from the concave side, severe stress concentration occurs on the inner surface near the arch base, while the stress at the top is concentrated on both sides of the arch crown. Under these dimensional conditions, the most probable failure mode of the bursting disc is shear failure along the edge at the location of the maximum Mises stress. This may cause fragments of the bursting disc to be flushed into the low-pressure zone, impairing the pressure relief performance. For this reason, cushion pads made of graphite, polytetrafluoroethylene (PTFE), aluminum or other materials are usually added to the pressure-bearing convex side of bursting discs in chemical pressure vessels. As shown in Fig. 8, both stress concentration regions are mitigated with the increase of initial thickness S_0, whereas the Mises stress on the inner surface near the arch base is consistently higher than that at the arch crown.

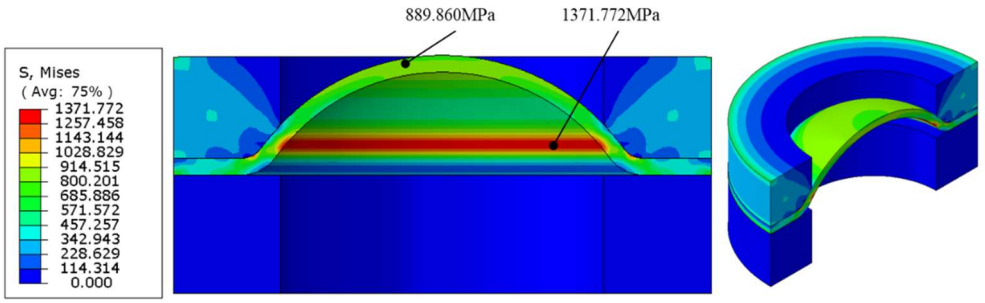

(a) Stress contour at S_0=0.5mm

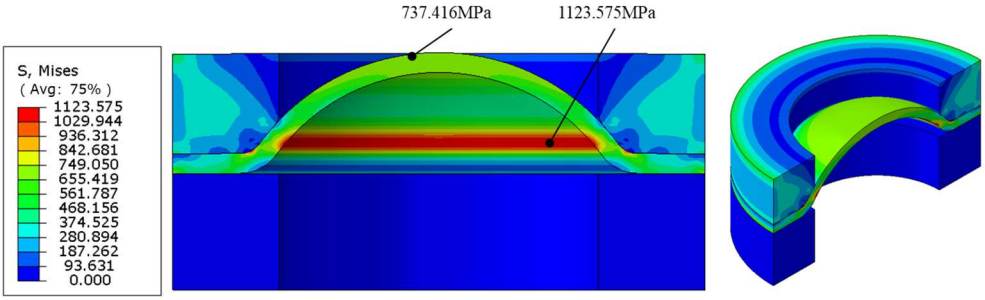

(b) Stress contour at S_0=0.6mm

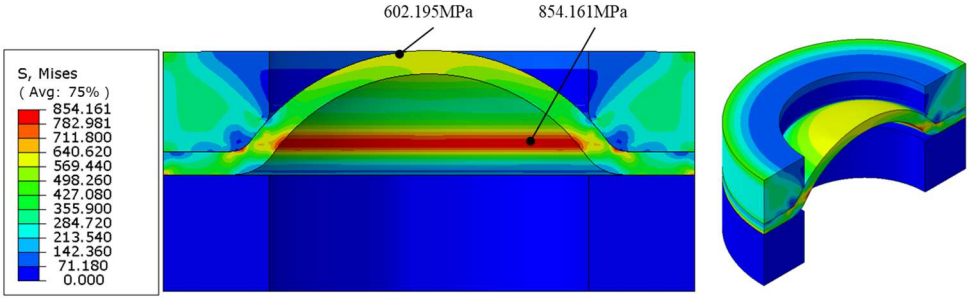

(c) Stress contour at S_0=0.7mm

ISSN: 2414-1895 DOI: 10.6919/ICJE.202605_12(5).0012

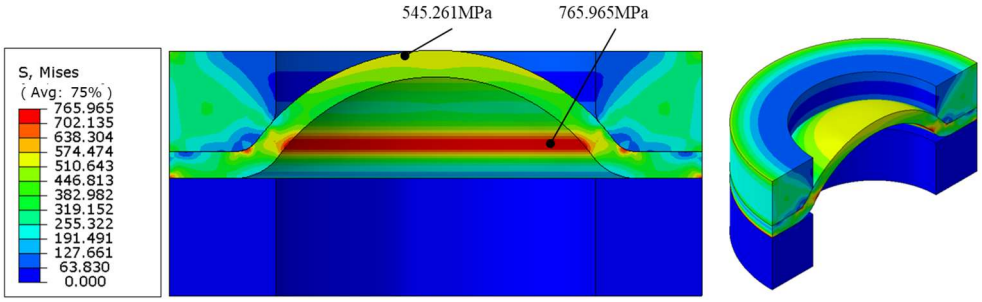

(d) Stress contour at S_0=0.8mm

Fig. 7 Effect of initial plate thickness S_0 on stress

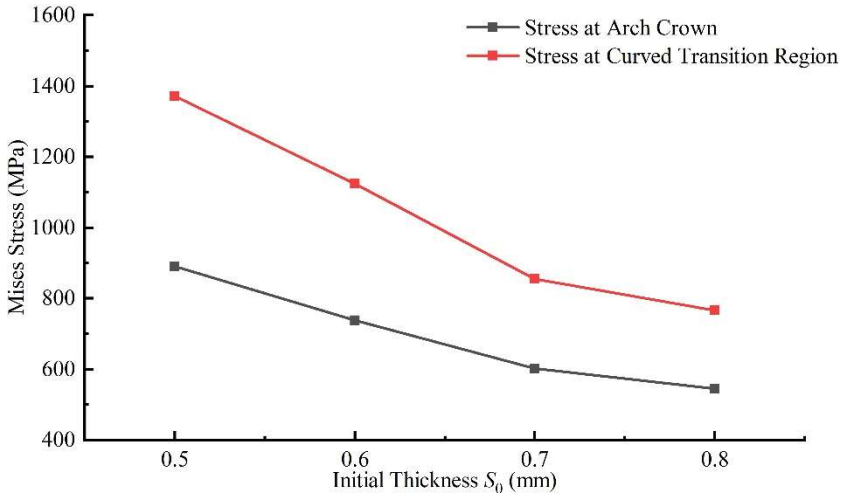

Fig. 8 Effect of initial plate thickness S_0 on stress at different locations

5.2 Effect of Bursting Disc Arch Height H on Stress

With other dimensional parameters fixed, the influence of arch height H on the stress distribution of the bursting disc was studied by varying H. Four values of H were adopted: 1.5 mm, 2.0 mm, 2.5 mm and 3.0 mm. The initial plate thickness S_0 was fixed at 0.7 mm, the major diameter of the bursting disc D at 11.2 mm, no top thinning was applied, the outer fillet R_{outer} at 0.7 mm, and the inner fillet R_{inner} at 1.4 mm. The simulation results are presented in Fig. 9. Stress concentration still occurs on the inner surface near the arch base. As the arch height H decreases, the stress concentration at the top shifts from both sides of the arch crown to the center of the arch crown. As shown in Fig. 10, both stress concentration regions are evidently alleviated with the increase of H, whereas the Mises stress on the inner surface near the arch base is consistently higher than that at the arch crown.

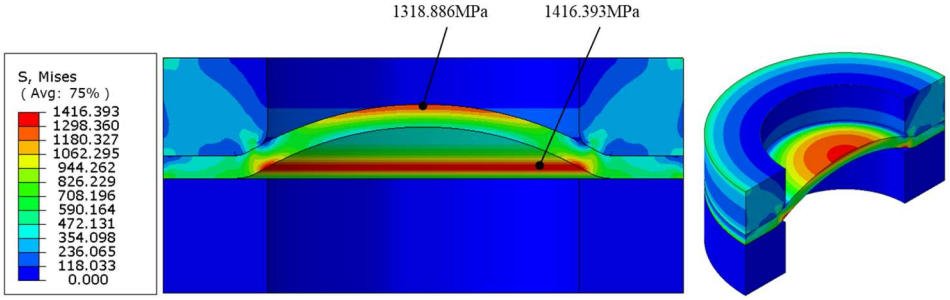

(a) Stress contour at H=1.5mm

ISSN: 2414-1895 DOI: 10.6919/ICJE.202605_12(5).0012

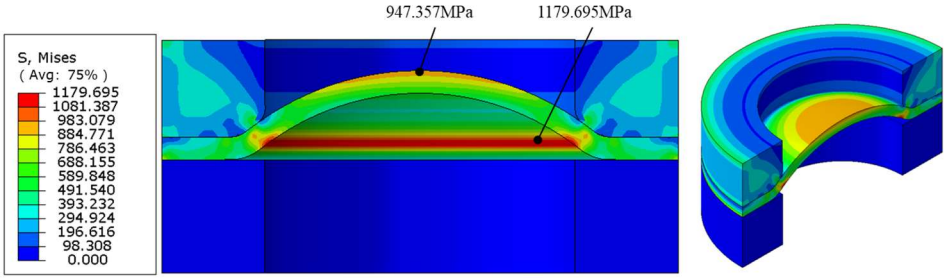

(b) Stress contour at H =2.0mm

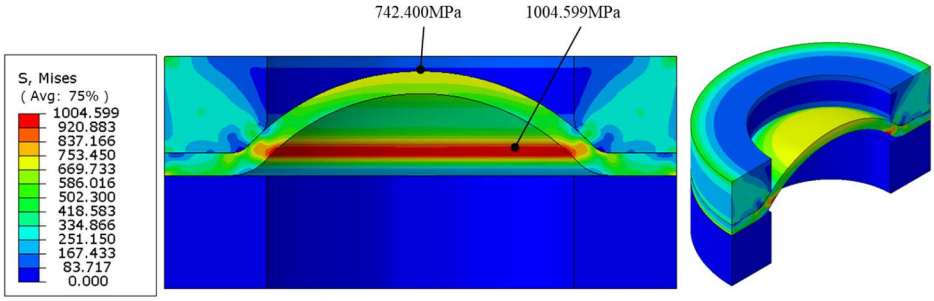

(c) Stress contour at H =2.5mm

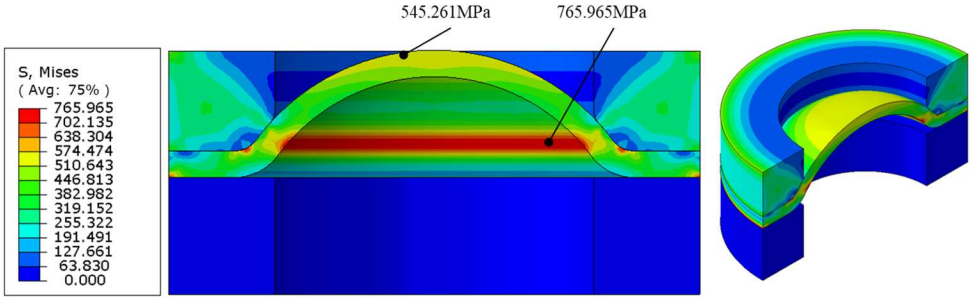

(d) Stress contour at H =3.0mm

Fig. 9 Effect of arch height H on stress

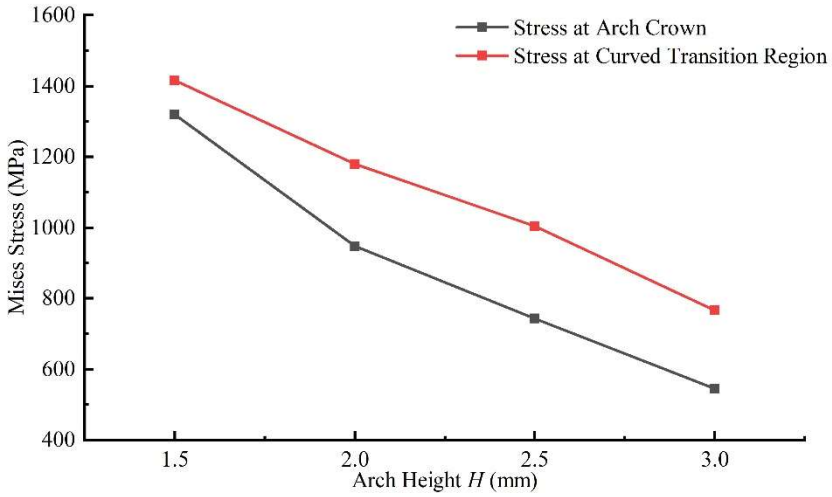

Fig. 10 Effect of arch height H on stress at different locations

5.3 Effect of Top Thinning Thickness t0 on Stress

With other dimensional parameters kept constant, the influence of top thickness on the stress distribution was investigated by thinning the top region to control the rupture location of the bursting disc. Four cases of top thinning thickness t_0 were adopted: 0.1 mm, 0.2 mm, 0.3 mm and no thinning.

ISSN: 2414-1895 DOI: 10.6919/ICJE.202605_12(5).0012

The arch height H was fixed at 3 mm, the initial plate thickness S_0 at 0.7 mm, the major diameter of the bursting disc D at 11.2 mm, the outer fillet R_{outer} at 0.7 mm, and the inner fillet R_{inner} at 1.4 mm. The simulation results are shown in Fig. 11 and Fig. 12. Stress concentration still occurs on the inner surface near the arch base. However, as the top thickness decreases, the stress concentration at the top is transferred from the inner surface near the arch base to the arch crown, and further concentrates on the inner surface of the arch crown. When the bursting disc cannot withstand the applied pressure, it first ruptures at the inner surface of the arch crown (the pole), and then tears irregularly along the clamping edge (the second stress concentration site, i.e., the inner surface of the arch base). This rupture trend is consistent with practical observations.

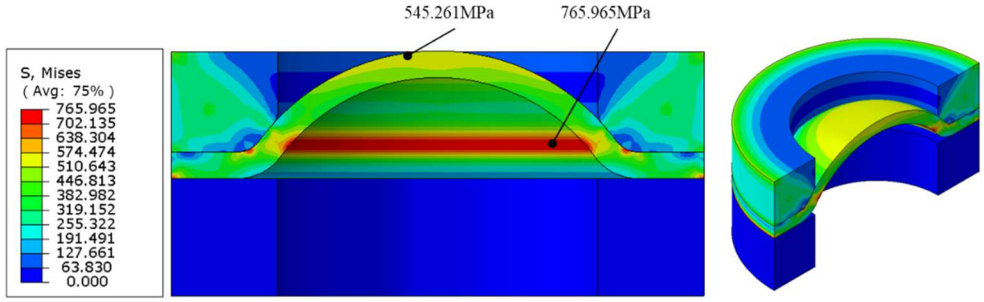

(a) Stress contour at t_0 =0mm

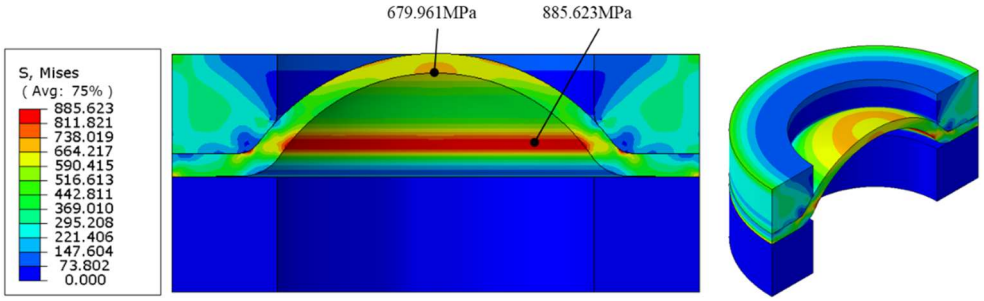

(b) Stress contour at t_0 =0.1mm

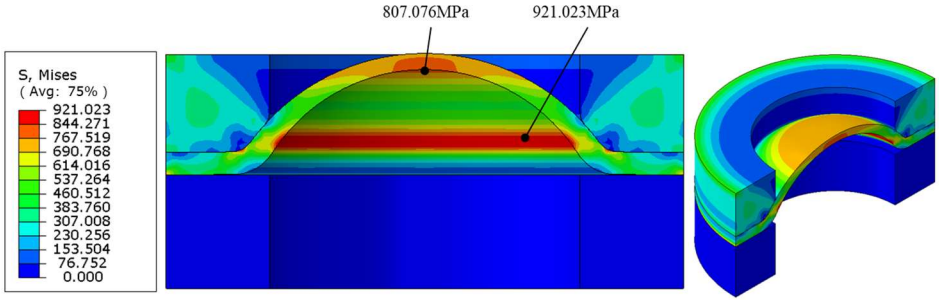

(c) Stress contour at t_0 =0.2mm

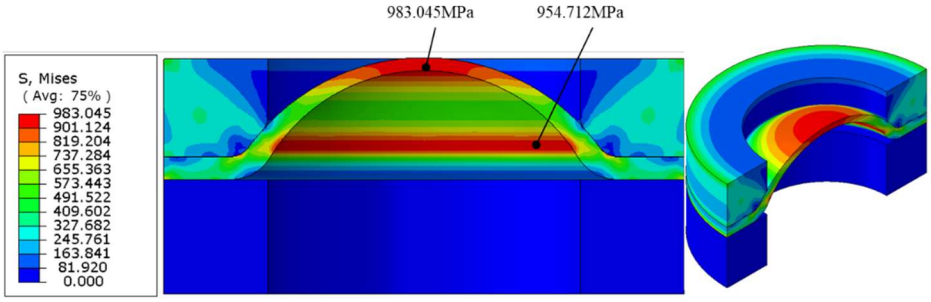

(d) Stress contour at t_0 =0.3mm

Fig. 11 Effect of top thinning thickness t_0 on stress

ISSN: 2414-1895 DOI: 10.6919/ICJE.202605_12(5).0012

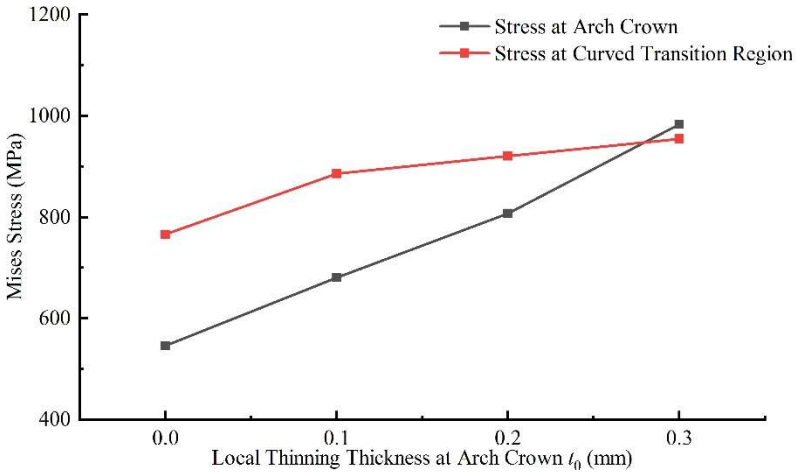

Fig. 12 Effect of top thinning thickness t_0 on stress at different locations

5.4 Effect of Temperature Variation on Burst Pressure

Temperature is a major external factor governing burst pressure. The influence of temperature on material properties has been examined in the foregoing sections, and the temperature-dependent performance of the developed 17.5k rupture disc is investigated in this part. Multiple simulation runs reveal that although temperature affects the Young's modulus of the material, the maximum Mises stress at 450 °F differs negligibly from that at 300 °F. Accordingly, the effect of temperature on the material yield strength is taken as the primary factor, and the yield strength is converted to burst pressure for analysis.

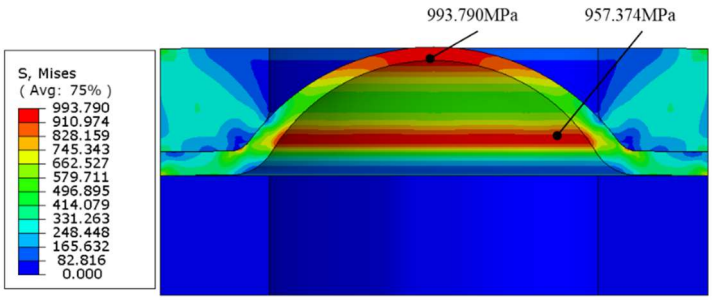

(a) Stress contour of the rupture disc at 17.5ksi

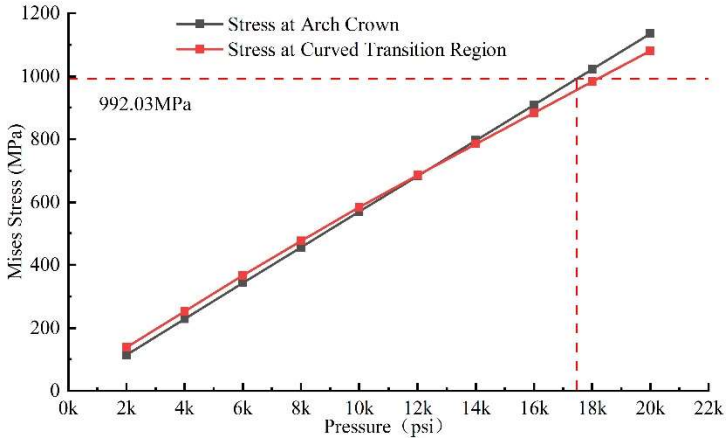

(b) Stress variation trend of the 17.5k rupture disc under different pressures

Fig. 13 Simulation results of the designed 17.5k rupture disc

ISSN: 2414-1895 DOI: 10.6919/ICJE.202605_12(5).0012

As presented in Fig. 13, the top thickness of the bursting disc is adjusted to control the maximum Mises stress at 17.5ksi at 993.790 MPa, which slightly exceeds the material yield strength of 992.03 MPa at 450 °F. The stress-pressure characteristics of the 17.5k rupture disc under varying pressures are then studied. As shown in Fig. 13(b), the stress concentration at the inner surface of the arch crown and the inner surface of the arch base increases nearly linearly with rising pressure. The maximum Mises stress occurs at the arch base under low pressure and migrates to the arch crown under high pressure, leading to an intersection between the stress-pressure curves of the two positions.

The burst pressure at each temperature is subsequently derived and fitted into a curve, as illustrated in Fig. 14. The curve can be approximated by the equation: y=0.0062x^2-6.5236x+19129. This trend is consistent with that of the 16K rupture disc manufactured by OSECO Corporation. It is inferred that the 16K rupture disc from OSECO employs Inconel 718 or a material with comparable performance as the raw material for the bursting disc.

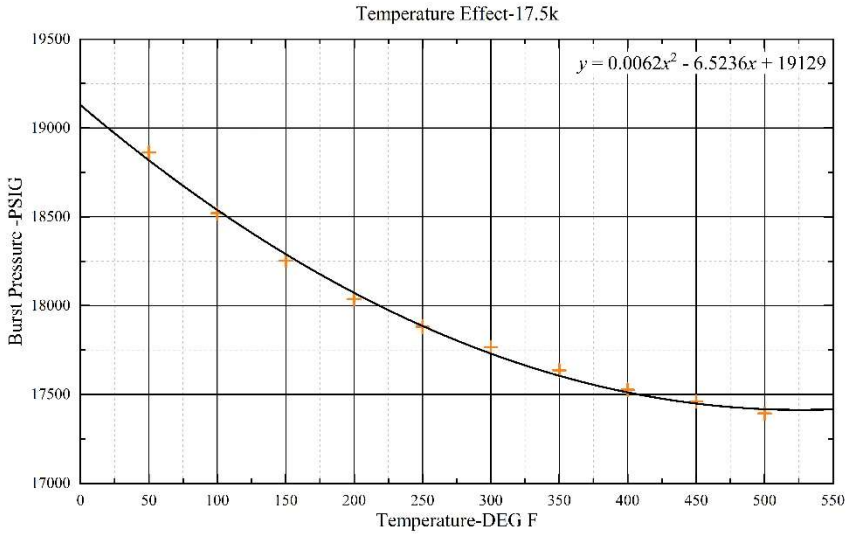

Fig. 14 Fitted temperature-burst pressure curve of the 17.5k rupture disc

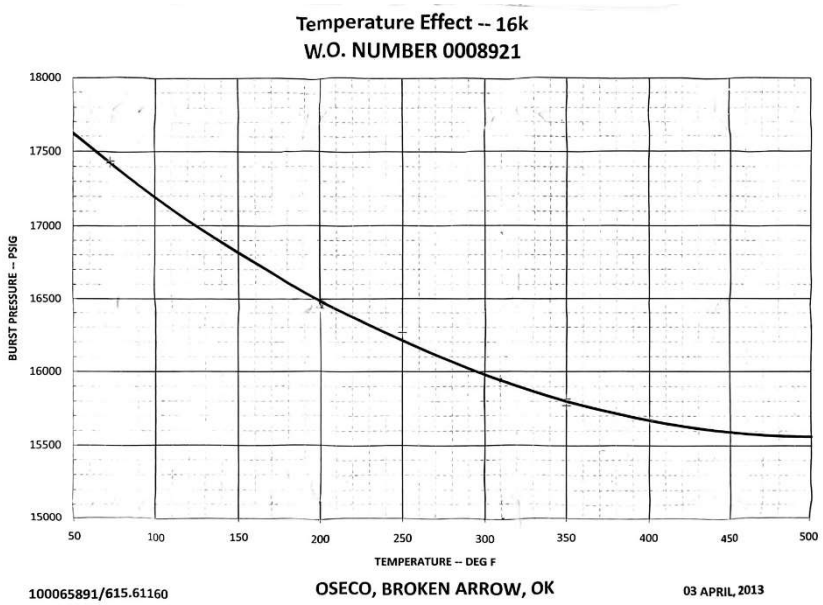

Fig. 15 Temperature-burst pressure curve of the 16K rupture disc manufactured by OSECO Corporation

ISSN: 2414-1895 DOI: 10.6919/ICJE.202605_12(5).0012

6. Conclusion

(1) Inconel 718 is an ideal candidate material for the bursting discs of APR rupture discs at present. Through material handbook analysis and temperature characteristic fitting, it is found that the nickel-based alloy Inconel 718 exhibits excellent yield strength retention, corrosion resistance and structural stability under high temperature, high pressure and H_2S/CO_2-containing medium environments. Its comprehensive performance is highly consistent with that of the materials used in the existing products of OSECO Company, providing a key material basis with practical feasibility for the research and development of domestic rupture discs.

(2) The geometric parameters of the bursting disc have a decisive influence on the burst pressure and failure mode. Based on the finite element simulation results of Abaqus, the increase of initial thickness S_0 and arch height H can both reduce the maximum Mises stress level and increase the burst pressure. Without the top thinning structure, the maximum stress concentration is mainly located on the inner surface of the arch bottom, which is prone to induce non-ideal shear failure along the edge. By setting a reasonable local thinning thickness t_0 at the arch top, the stress concentration area can be successfully transferred to the inner surface of the arch top, making the bursting disc initiate cracking preferentially at the pole position. Its failure mode is highly consistent with the failure morphology of OSECO products in practical engineering. This conclusion indicates that the top thinning structure is a key design means to achieve controllable rupture and improve pressure relief reliability.

(3) The influence of temperature on the burst pressure of the rupture disc is mainly reflected through the yield strength of the material. The simulation results show that in the temperature range of 300-450°F, the effect of temperature change on Young's modulus contributes little to the overall stress level, while the decrease of material yield strength with temperature is the dominant factor leading to the reduction of burst pressure. The temperature-burst pressure relationship curve of the designed 17.5kPsi rupture disc is consistent with the trend of similar products of OSECO Company, which further verifies the rationality of material selection and structural design.

References

[1] Jeong, J.Y., Lee, J., Yeom, S. et al. A study on the grooving process of a cross-scored rupture disc. Int. J. Precis. Eng. Manuf. 2012, Vol. 13, p. 219-227.

[2] Nwaoha, C. Appendix IV: Rupture Disk Selection. In Process Plant Equipment: Operation, Control, and Reliability. John Wiley & Sons, Inc., 2012, p. 665-668.

[3] Liu, Z.X., Zhou, D.M., Xu, H. et al. Experimental and numerical investigation of burst characteristics of ultra-high pressure rupture discs. Int. J. Press. Vessel. Pip. 2025, Vol. 215, p. 105455.

[4] GB 567.1-567.4-2012. Bursting Disc Safety Devices. Standards Press of China, 2013.

[5] Gong, L., Duan, Q.L., Liu, J.L. et al. Effect of burst disk parameters on the release of high-pressure hydrogen. Fuel 2019, Vol. 235, p. 485-494.

[6] Schrank, M. Investigation on the degradation and opening behavior of knife blade burst disks. J. Loss Prev. Process Ind. 2014, Vol. 32, p. 161-164.

[7] Tao, L.B., Yang, Q.X., Xu, H. et al. Demonstration and calculation of rupture discs in vacuum vessel pressure suppression system of CFETR. Nucl. Fusion Plasma Phys. 2020, Vol. 40 (No. 2), p. 162-167.

[8] Yang, C., Hui, H., Huang, S. Comparative Study on Theoretical Calculation and Numerical Simulation of Designed Bursting Pressure of Ultrahigh Pressure Bursting Discs. Pressure Vessel Technol. 2020, Vol. 37 (No. 3), p. 21-26, 40.

[9] Wang, C.F., Xu, G., Man, M. et al. Research on parameter characteristics of reverse domed scored bursting disc. Vacuum Cryogen. 2021, Vol. 27 (No. 5), p. 485-489.

[10] Lei, W.Q., Zhang, K., Zhang, J.X. Failure Analysis of Tube Leakage in Heat Exchange Tube of Coiled Tubular Heat Exchanger. 2018 Gansu Welding Academic Conference, Lanzhou, China, 2018.

[11] Bian, Z.C., Li, M.Y., Liu, H.X. et al. Comprehensive optimization of tensile and creep properties of Inconel 718 superalloy at room temperature and elevated temperature through grain boundary engineering treatments. Mater. Sci. Eng. A 2026, Vol. 959, p. 150051.

ISSN: 2414-1895 DOI: 10.6919/ICJE.202605_12(5).0012

[12] Xiong, A.J., Yang, J., Song, Y. et al. Research on Rupture Disc Test and Rupture Pressure Model for Oil and Gas Wells. Pressure Vessel Technol. 2017, Vol. 34 (No. 8), p. 1-6.

[13] Kong, X.W., Zhang, J.C., Li, X.Q. et al. Experimental and finite element optimization analysis on hydroforming process of rupture disc. Procedia Manuf. 2018, Vol. 15, p. 892-898.